UPPSALA
UNIVERSITET

Digital Comprehensive Summaries of Uppsala Dissertations from the Faculty of Science and Technology 1132

Studies of Single and Multiple Ionization Processes in Rare Gases and some Small Molecules

LAGE HEDIN

ACTA
UNIVERSITATIS
UPSALIENSIS
UPPSALA
2014

ISSN 1651-6214
ISBN 978-91-554-8910-6
urn:nbn:se:uu:diva-221128

Dissertation presented at Uppsala University to be publicly examined in sal 80121, Ångströmlaboratoriet, Lägerhyddsvägen 1, Uppsala, Friday, 16 May 2014 at 13:15 for the degree of Doctor of Philosophy. The examination will be conducted in Swedish. Faculty examiner: Professor Dag Hanstorp (Göteborgs universitet).

Abstract

Hedin, L. 2014. Studies of Single and Multiple Ionization Processes in Rare Gases and some Small Molecules. *Digital Comprehensive Summaries of Uppsala Dissertations from the Faculty of Science and Technology* 1132. 55 pp. Uppsala: Acta Universitatis Upsaliensis. ISBN 978-91-554-8910-6.

In this thesis various aspects of photoionization are investigated with respect to both single and multiple electron emission from atoms and molecules. The studies include both valence and core levels and involve transitions which leave the atoms or molecules in various charge states.

S2p electrons in the CS_2 molecule were excited into Rydberg orbitals close to the ionization threshold. Subsequent autoionization leads to the emission of single electrons which were detected by a conventional electron spectrometer, bringing the molecule into various cationic states characterized by two valence holes and a Rydberg spectator electron. Vibrational progressions have been assigned as excitations of the totally symmetric ν_1 and the asymmetric stretching ν_3 modes in the cationic states.

Double ionization spectra of the CS_2 molecule were recorded in the S2p and C1s innershell ionization regions using a magnetic bottle many-electron coincidence spectrometer, revealing dicationic states formed out of one inner-shell vacancy and one vacancy in the valence region. The spectrum connected to the S2p vacancy is richly structured in contrast to the spectrum connected to the C1s vacancy, which shows essentially one distinct band.

The development of a new variant of the magnetic bottle coincidence technique tailored for valence triple photoionization studies of rare gas atoms at synchrotron radiation sources is presented, overcoming the problem of high repetition rate in single-bunch operation of the storage ring. The studies of the rare gas atoms confirm that a correction of the lowest triple-ionization energy of Kr, currently listed in standard tables, is needed.

Also, single-site N1s and O1s double core ionization of the NO and N_2O molecules and single-site O1s, C1s and S2p double core ionization of the OCS molecule has been studied with the magnetic bottle technique. Double core holes are of particular interest due to putatively larger chemical shifts compared to single core holes. The observed ratio between the double and single ionization energies are in all cases close or equal to 2.20.

Lage Hedin, Department of Physics and Astronomy, Molecular and condensed matter physics, Box 516, Uppsala University, SE-751 20 Uppsala, Sweden.

ISSN 1651-6214
ISBN 978-91-554-8910-6
urn:nbn:se:uu:diva-221128 (http://urn.kb.se/resolve?urn=urn:nbn:se:uu:diva-221128)

To Carina

List of papers

This thesis is based on the following papers, which are referred to in the text by their Roman numerals.

I **An x-ray absorption and a normal Auger study of the fine structure in the S2p^{-1} region of the CS_2 molecule**
L. Hedin, J.H.D Eland, L. Karlsson and R. Feifel
J. Phys. B: At. Mol. Opt. Phys. **42**, 085102 (2009)

II **Cationic Rydberg states observed in resonantly enhanced electron spectra of CS_2**
L. Hedin, J.H.D. Eland, L. Karlsson, and R. Feifel
Chem. Phys. **355**, 55 (2009)

III **Core-valance double photoionization of the CS_2 molecule**
E. Andersson, J. Niskanen, L. Hedin, J.H.D. Eland, P. Linusson, L. Karlsson, J.-E. Rubensson, V. Carravetta, H. Ågren and R. Feifel
J. Chem. Phys. **133**, 094305 (2010)

IV **Coincidence technique using synchrotron radiation for triple photoionization: Results on rare gas atoms**
J.H.D. Eland, P. Linusson, L. Hedin, E. Andersson, J.-E. Rubensson, and R. Feifel
Phys. Rev. A **78**, 063423 (2008)

V **N1s and O1s double ionization of the NO and N_2O molecules**
L. Hedin, M. Tashiro, P. Linusson, J.H.D. Eland, M. Ehara, K. Ueda, V. Zhaunerchyk, L. Karlsson, K. Perneståal, and R. Feifel
J. Chem. Phys **140**, 044309 (2014)

VI **Single site double core level ionization of OCS**
L. Hedin, M. Tashiro, P. Linusson, J.H.D. Eland, M. Ehara, K. Ueda, V. Zhaunerchyk, L. Karlsson, and R. Feifel
Chem. Phys., submitted (March 15, 2014)

Reprints were made with permission from the publishers.

The following is a list of papers not included in the thesis.

- **Single-photon core-valence double ionization of molecular oxygen**
  E. Andersson, M. Stenrup, J.H.D. Eland, L. Hedin, M. Berglund, L. Karlsson, Å. Larson, H. Ågren, J.-E. Rubensson, and R. Feifel
  Phys. Rev. A **78**, 023409 (2008)

- **Spectra of the triply charged ion CS_2^{3+} and selectivity in molecular Auger effects**
  J.H.D. Eland, C. Rigby, E. Andersson, J. Palaudoux, L. Andric, F. Penent, P. Linusson, L. Hedin, L. Karlsson, J.-E. Rubensson, Y. Hikosaka, K. Ito, P. Lablanquie and R. Feifel
  J. Chem. Phys. **132**, 104311 (2010)

- **Complete double valence photoionization study of the electron spectra of krypton**
  P. Linusson, L. Hedin, J.H.D. Eland, R.J. Squibb, M. Mucke, S. Zagorodskikh, L. Karlsson, and R. Feifel
  Phys. Rev. A **88**, 022510 (2013)

- **Multi-electron coincidence study of the double Auger decay of 3d ionised krypton**
  E. Andersson, S. Fritzsche, P. Linusson, L. Hedin, J.H.D. Eland, J.-E. Rubensson, L. Karlsson, and R. Feifel
  Phys. Rev. A **82**, 043418 (2010)

- **Triple ionisation of methane by double Auger and related pathways**
  J.H.D. Eland, P. Linusson, L. Hedin, E. Andersson, J.-E. Rubensson and R. Feifel
  Chem. Phys. Lett. **485**, 21 (2010)

- **Triple ionization spectra by coincidence measurements of double Auger decay: The case of OCS**
  J.H.D. Eland, M. Hochlaf, P. Linusson, E. Andersson, L. Hedin, and R. Feifel
  J. Chem. Phys. **132**, 014311 (2010)

- **Experimental and theoretical study of core-valence double photoionization of OCS**
  J. Niskanen, V. Carravetta, O. Vahtras, H. Ågren, H. Aksela, E. Andersson, L. Hedin, P. Linusson, J.H.D. Eland, L. Karlsson, J.-E. Rubensson, and R. Feifel
  Phys. Rev. A **82**, 043436 (2010)

- **Double ionization of atomic cadmium**
  P. Linusson, S. Fritzsche, J.H.D. Eland, L. Hedin, L. Karlsson and R. Feifel
  Phys. Rev. A **83**, 023424 (2011)

- **Triple ionization of CO_2 by valence and inner shell photoionization**
  J.H.D. Eland, L. Andric, P. Linusson, L. Hedin, S. Plogmaker, J. Palaudoux, F. Penent, P. Lablanquie and R. Feifel
  J. Chem. Phys. **135**, 134309 (2011)

- **Influence of double Auger decay on low-energy 3d photoelectrons of Krypton**
  S. Sheinerman, P. Linusson, J.H.D. Eland, L. Hedin, E. Andersson, J.-E. Rubensson, L. Karlsson, and R. Feifel
  Phys. Rev. A **86**, 022515 (2012)

- **Single and multiple photoionisation of H_2S by 40 - 250 eV photons**
  J.H.D. Eland, R.F. Fink, P. Linusson, L. Hedin, S. Plogmaker and R. Feifel
  Phys. Chem. Chem. Phys. **13**, 18428 (2011)

- **Formation of Kr^{3+} via core-valence doubly ionized intermediate states**
  E. Andersson, P. Linusson, S. Fritzsche, L. Hedin, J.H.D. Eland, L. Karlsson, J.-E. Rubensson, and R. Feifel
  Phys. Rev. A **85**, 032502 (2012)

- **Symmetry breaking in core-valence double photoionization of SO_2**
  J. Niskanen, E. Andersson, J.H.D. Eland, P. Linusson, L. Hedin, L. Karlsson, R. Feifel, and O. Vahtras
  Phys. Rev. A **85**, 023408 (2012)

Author's contribution

Experimental physics is a collaborative effort and the works presented in this thesis are in part and in various ways due to my own achievements as explained in the following sentences. I have taken part in all the experiments presented, except those of papers I and II which were carried out at the MAX-II laboratory in Lund. I have done the data analyses for papers I, II, V and VI and participated in the writing of all publications. In particular, I have developed new computer software for detailed analysis of the multi-coincidence time-of-flight data collected in some of the experiments, and made complete data analyses of the experimental results reported in papers V and VI using these programs.

Contents

1. Introduction

Single photon absorption by atoms or molecules in gas, liquid or condensed phase, can lead to the ejection of one or several electrons per event, promoting the system into a singly or more highly charged state. The basic experimental technique for analyzing the kinetic energy of a liberated electron is photoelectron spectroscopy as developed in the 1950's by Prof. Kai Siegbahn and his group at Uppsala University [1, 2]. It gives important information on the electronic structure and related dynamics of the system studied. If more than one electron is released per photoabsorption event, the complete kinetic energy analysis requires coincidence experiments as pioneeringly introduced to this research field and developed by Prof. John H.D. Eland at Oxford University, United Kingdom [3].

The main topics of this thesis concern the identification of Rydberg states in the inner valence region of singly-ionized CS_2 as well as studies of core-valance doubly ionized CS_2. The development of an experimental technique for valence triple photoionization studies is exemplified for rare gas atoms as well as for double core holes in the NO, N_2O and OCS molecules. Soft X-ray photons provided by two different synchrotron light sources, the MAX-laboratory in Lund, Sweden, and BESSY-II in Berlin, Germany, have been used for these studies. The author of this thesis has primarily used beamline U49/2 PGM-2 [4] at the BESSY-II [5] storage ring in Berlin and the magnetic bottle coincidence spectrometer for data recording, and descriptions of these devices will be given in section 3. The concept of using magnetic bottle spectrometers [6] for the coincidence experiments was recently developed by J. H. D. Eland [7, 8].

In the electron spectra of the CS_2 molecule many new electron bands are observed which reflect states in the cation that are close to the electronic states of the dication. These new states are identified in making use of the results of recent double ionization electron spectroscopy works on CS_2 by Eland [9]. The present studies were carried out by resonantly exciting sulphur 2p electrons into neutral intermediate Rydberg states, which subsequently decay into cationic states via electron emission. Prior to the recording of these resonantly excited electron spectra, photoabsorption spectra were measured in the vicinity of the sulphur 2p edge in order to map out the pre-edge resonances including Rydberg states. Due to the high photon energy resolution employed in the present work in comparison to previous studies, new spectral features were revealed in these recordings which are assigned in this thesis.

Double photoionization spectra of the CS_2 molecule were recorded in the S2p and C1s inner-shell ionization regions and reflect dicationic states formed

out of one inner-shell vacancy and one vacancy in the valence region. The experiments were carried out using a multi-electron-coincidence spectrometer based on the magnetic bottle principle [6]. Coincidence measurements of the flight times of two emitted electrons using ionizing synchrotron ring light pulses as time reference were performed.

The experimental technique for the studies of triple photoionization is based on coincidence measurement of the flight times of all three emitted electrons captured in a magnetic bottle as well as the flight time of the created ion detected in a mass spectrometer. Provided that the ion flight time is known from independent calibration of the mass spectrometer, it can be used to identify the ionizing synchrotron ring light pulses. This removes any ambiguity in the time to energy conversion and suppresses strongly the background of false coincident electron triples.

Single site N1s and O1s double core ionization of the NO and N_2O molecules and single site C1s, O1s and S2p double core ionization of the OCS molecule has been studied using the same multi-electron-coincidence spectrometer mentioned in connection with double ionization. These studies are based on coincidence measurements of the flight times of four emitted electrons, two primary photoelectrons and two secondary Auger electrons. The energies obtained for the double core holes as well as Auger electron spectra of N_2O and OCS are reported in this thesis. Large chemical shifts are observed which suggest that reorganization of the electrons upon double core ionization is significant. The ratio between the double and single core ionization energies are in all cases close or equal to 2.20.

2. Electronic Structure and Photoionization

2.1 Photoelectron Spectroscopy

Photoelectron spectroscopy is based upon photoionization (see Fig 2.1) of a sample and detection of the liberated electrons by means of a kinetic energy analyzer. In such an instrument, the kinetic energies E_{kin} of the released electrons are measured, and from these energies the binding energies E_B can be determined according to Einstein's photoelectric law, which is the theoretical basis for the emission of electrons upon photon impact. Einstein's photoelectric law is denoted as

$$E_{kin} = h\nu - E_B \tag{2.1}$$

where h is Planck's constant and ν is the frequency of the electromagnetic radiation. The kinetic energy of the electrons as measured by photoelectron spectroscopy gives important information on the energy levels in atoms or molecules. Using well defined monochromatic radiation, the binding energy E_B of the electron can be determined from measured kinetic energy E_{kin}. In

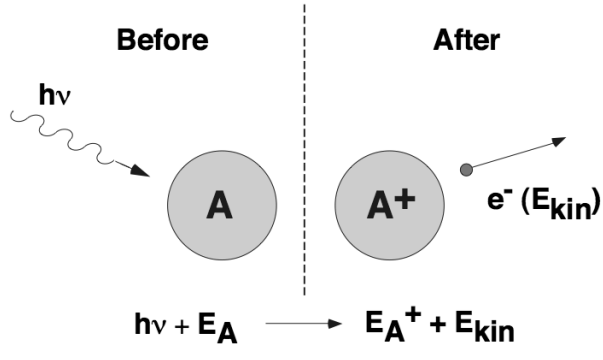

Figure 2.1. Schematic drawing illustrating photoionization (courtesy of our research group).

the *non-resonant or direct photoionization* process electrons are emitted in the primary process, leaving the ionized atoms or molecules in charged states. Starting with a system initially in the neutral ground state (see Fig 2.1), the simplest final state will be a singly ionized state, which can be described by

$$E_{kin} = E(A) + h\nu - E(A^+) \tag{2.2}$$

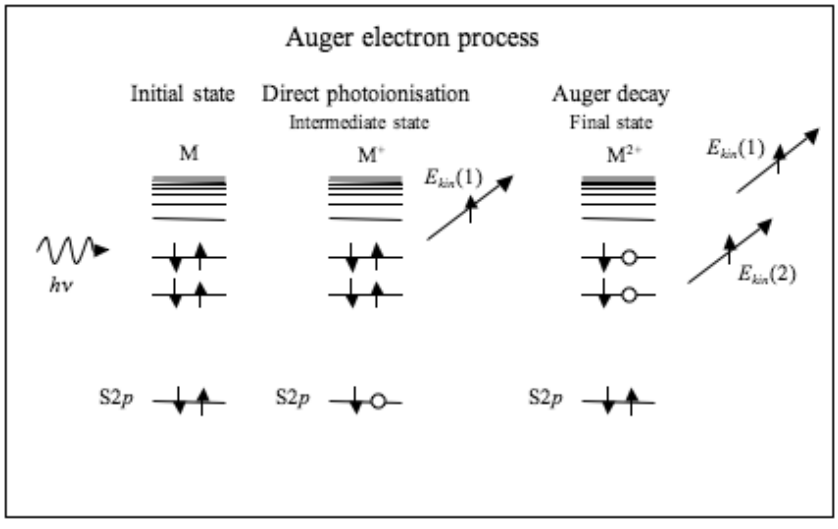

Figure 2.2. Schematic drawing showing transitions involved in the normal Auger process when induced by electromagnetic radiation.

where $E(A)$ is the energy of the neutral ground state and $E(A^+)$ the energy of the singly charged state created. Equations 2.1 and 2.2 give

$$E_B = E(A^+) - E(A) \tag{2.3}$$

In the resonant or photoexcitation process an electron is excited to an unoccupied orbital, and the process can be denoted as

$$E(A^*) = E(A) + h\nu \tag{2.4}$$

where $E(A^*)$ is the energy of the excited electronic state. If the photon energy is sufficiently high, an inner-shell vacancy can be created. One way for the system to lower its energy is to eject an electron and emerge into a charged state. In that case an outer valence electron fills the vacancy in the inner shell region and energy will be released. Another electron, typically from the outer valence region, can retrieve this energy and leave the system. If the molecule, for example, in the excited electronic state is non-charged, it may decay to a singly charged ion. The process is generally called *autoionization* or *resonant Auger decay* and the kinetic energy of the electron is obtained from

$$E_{kin} = E(A^*) - E(A^+) \tag{2.5}$$

The processes that may be involved are further described in the next section. If the excited electronic state is singly charged, the decay may lead to a doubly charged ion and this process is known as normal Auger decay (cf. Fig 2.2)

$$E_{kin} = E(A^+) - E(A^{2+}). \tag{2.6}$$

2.2 Non-resonant and Resonant Photoionization

In conventional photoelectron spectroscopy the photon energy is often such that it does not fit to an excited state of the system, and the photoionization can be considered mainly as a direct process (Fig. 2.3, upper part). This is the typical situation if one uses HeI and HeII radiation, as for example, provided by UV gas discharge line-sources, as if one chooses at a synchrotron radiation beam line the photon energy to exceed a specific ionization threshold.

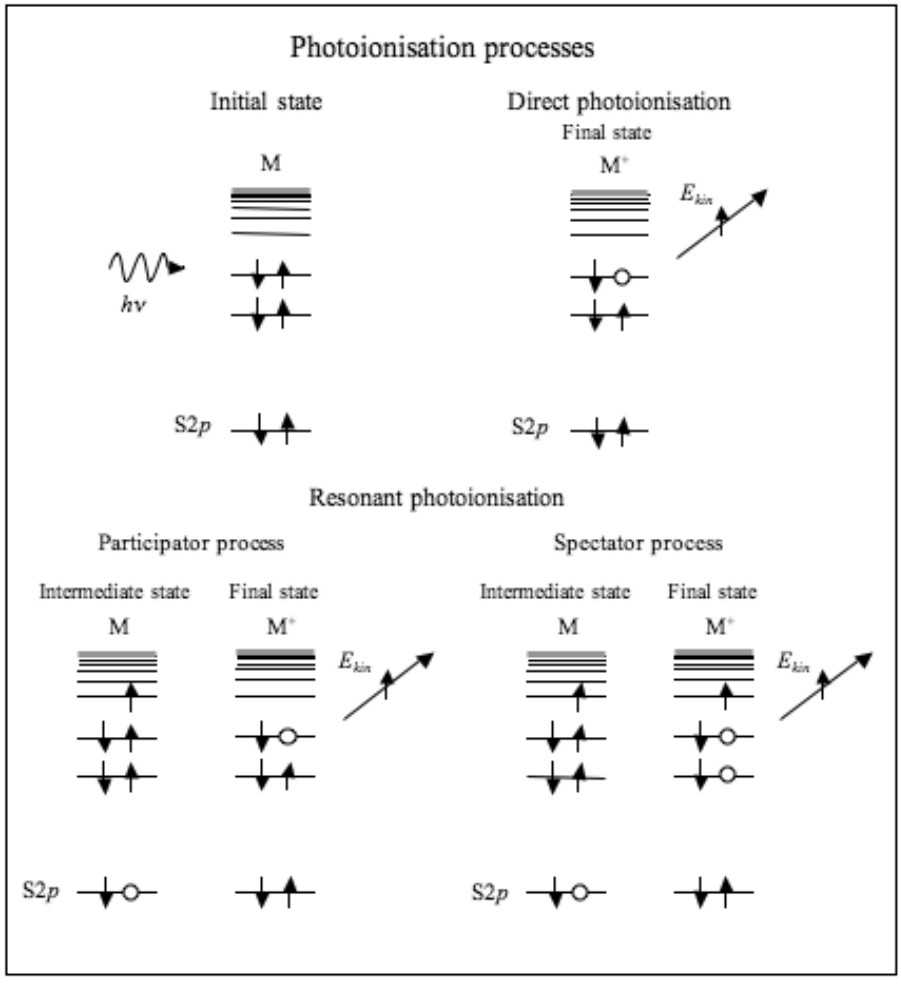

Figure 2.3. Schematic drawing showing direct and resonant photoionization processes.

Since the photon energy can be varied easily at synchrotron radiation beam lines, it may be deliberately chosen in order to coincide with a neutral intermediate electronic state of the system studied. In this case the direct process

is not the only possible channel for photoionization, but in addition, a resonant process can take place where the system is transferred into a neutrally excited intermediate excited electronic state. Subsequently the system may become deexcited via autoionization. The final electronic states reached are in the cation, just like for the direct process (see Fig. 2.3, lower part), but since an intermediate state is involved in the resonant process, the probability for populating the cationic states can be expected to be different. In principle, two different types of deexcitation processes can be distinguished, participator and spectator (se Ref. [10] and refs. therein). In the former type of process, the excited electron takes actively part in the decay, whereas in the latter type of process the excited electron remains in the valence orbital and another one fills the inner shell hole whereby the released energy gets transferred to a third electron leaving the system.

In the present investigation (Paper II) the photoionization experiments have been carried out under such resonant conditions. The resonant energies are chosen to correspond with excitation from S2p levels to the $4s\sigma_g$ Rydberg state [11] only a few eV below the ionization limit. In this level the excited electron tends to remain (spectator process) whereas the autoionization process involves electrons from outer valence shells and, thereby, many new highly excited inner valence cationic states are reached. In fact, it seems that these states are the same as the valence states of the dication with the exception for the presence of the $4s\sigma_g$ Rydberg (spectator) electron. Thus, the resonant spectra resemble very much, even quantitatively, the double photoionization and normal Auger electron spectra. Auger electron transitions are conventionally referred to as "normal" in processes where the deexcitation of a cationic state leads to emission of a second electron and the consequent formation of a dication.

2.3 Franck-Condon Principle

In a molecule, the nuclei normally move slowly compared to the electronic motion, which is the basis of the Frank-Condon-principle [12]. Within the Born-Oppenheimer approximation [13] the transition moment can be described as a product of an electric dipole matrix element and a vibrational overlap integral

$$\vec{R} = \langle \psi'_{el} | \mu_{el} | \psi''_{el} \rangle \langle \psi'_{vib} | \psi''_{vib} \rangle = \vec{R}_{el} \langle \psi'_{vib} | \psi''_{vib} \rangle \tag{2.7}$$

where ψ' and ψ'' are the final and initial states, respectively, and μ_{el} is the electronic transition moment. The transition probabilities, and the associated peak intensities, are proportional to the square of $\vec{R}$, where the square of the vibrational overlap integral is known as the Frank-Condon factor. By this the Frank-Condon factor becomes a measure of the molecular geometry difference between the initial and final states, i.e. a measure of the difference in

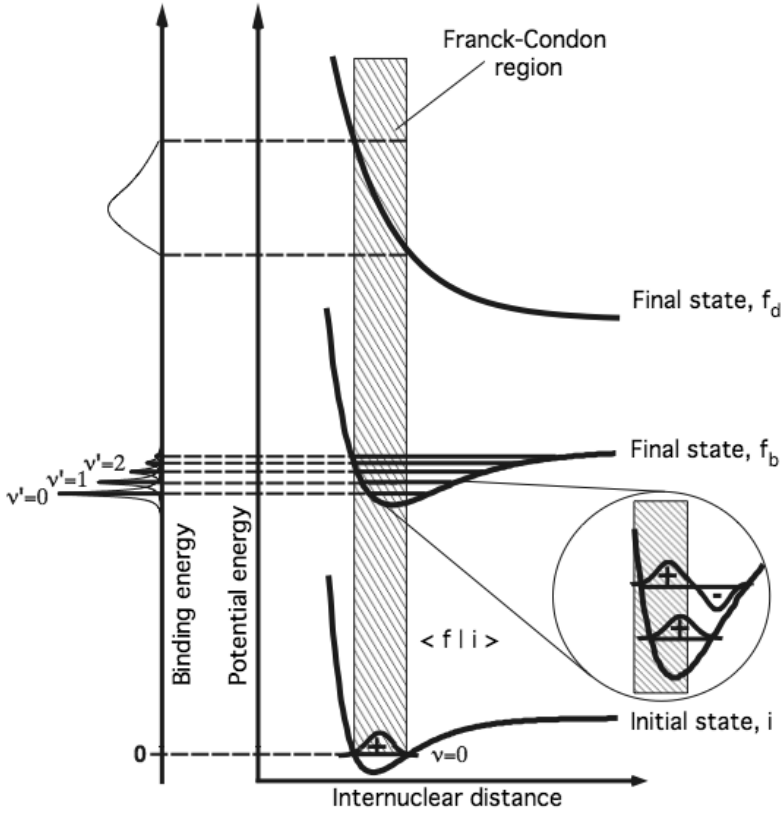

Figure 2.4. Final states (f_b and f_d) represent a bound state (f_b) and a dissociative state (f_d) of the singly ionized molecule. (courtesy of our research group).

equilibrium bond distance between the initial and final states of a diatomic molecule, see Fig 2.4 where the lower potential curve (Initial state, i) in the figure represents the neutral ground state and the upper curves (Final state, f_b and f_d) represent a single ionizated bound final state (f_b) and a dissociative final state (f_d).

If a hole is created in a bonding (antibonding) orbital the strength in the bonding (antibonding) decreases (increases) and the equilibrium bond distance tends to increase (decrease) so $r_e^{'} > r_e^{''}$ ($r_e^{'} < r_e^{''}$) where $r_e^{'}$ and $r_e^{''}$ are the equilibrium bond distances in the final and initial states, respectively. This can give rise to extensive vibrational progressions where the most intensive peak is not necessarily the energetic lowest one and the vibrational energies may differ considerably from those of the initial state. If, on the other hand, a hole is created in a non-bonding orbital it normally has little influence on the molecular

geometry and $r_e' \approx r_e''$. In this case transitions mostly take place between the vibrationless states with weakly excited overtones in short progressions and the vibrational energies are with small differences the same as those in the initial state. Qualitative arguments of this kind are used in the present work, in particular in Papers I and II, to draw conclusions about orbital characters and stability of various electronic states.

2.4 Electron Correlation Effects

Usually, in the outer valence region there is a one-to-one correspondence between molecular orbitals and the strong lines in a photoelectron spectrum. Electron correlation allows single-hole configurations to interact with two-holes-one-particle-excited configurations, often referred to as satellite states. Some of the intensity associated with the single-hole states may be redistributed among several satellite states, and in many cases main lines in the inner valence region representing the single-hole state can no longer be distinguished due to this interaction. This is known as a breakdown of the single particle model of ionization [14]. This breakdown effect is usually encountered for electrons with ionization potentials from about 20 to about 50 eV and this is the case also in the present study (Papers I and II).

2.5 Single Photon Multi-ionization

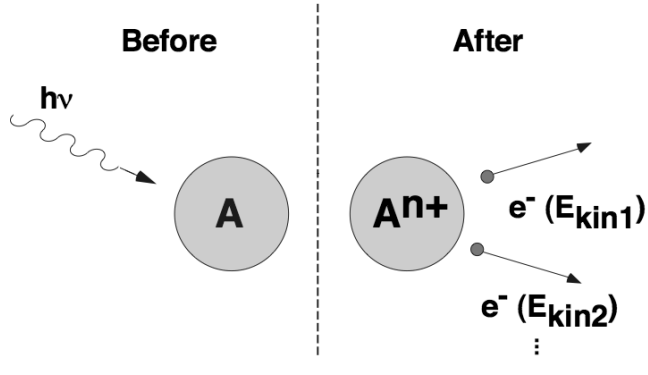

Figure 2.5. Schematic illustration of single-photon multi-ionization (courtesy of our research group).

As mentioned in the introduction, single photon absorption can lead to the ejection of more than one electron, which is schematically illustrated in Fig. 2.5. E.g. the normal Auger decay can be considered as a prominent case of

such a process. Accordingly, the photoelectric law needs to be extended, and one can write formerly:

$$E_{B1} + E_{B2}(+\ldots) = h\nu - E_{kin1} - E_{kin2}(-\ldots) \tag{2.8}$$

The sum on the left hand side of eq.2.8 defines the double (multiple) ionization energy. Upon single photon absorption, the release of two or more electrons, whether directly or in a sequential manner, is due to electron correlations, and the simultaneous detection of all particles will give detailed insights into the underlying relations among the electrons. The coincident detection of several particles requires a highly efficient tool, like, e.g., the so-called Time-Of-Flight PhotoElectron-PhotoElectron COincidence (TOF-PEPECO) technique developed by Prof. John H.D. Eland at Oxford University, UK [7] (see also chapter 3.5.1). This technique is used in the studies presented in papers III, V and VI. A variant of this technique is discussed in Paper IV of this thesis (see also chapter 3.5.2).

3. Experimental Techniques and Instrumentation

3.1 Monochromatic Synchrotron Radiation

Upon acceleration, charged particles emit radiation according to the laws of electrodynamics. When the particles travel in a curved trajectory the emitted radiation reaches maximum intensity in the direction perpendicular to the acceleration whereas it is zero along the acceleration direction. This is true as long as the velocity of the charged particles is low compared to the velocity of light. At higher velocity of the charged particles relativistic influences become more important. In the laboratory (observer) frame the radiation is emitted as a narrow cone tangentially to the velocity of the particle [15].

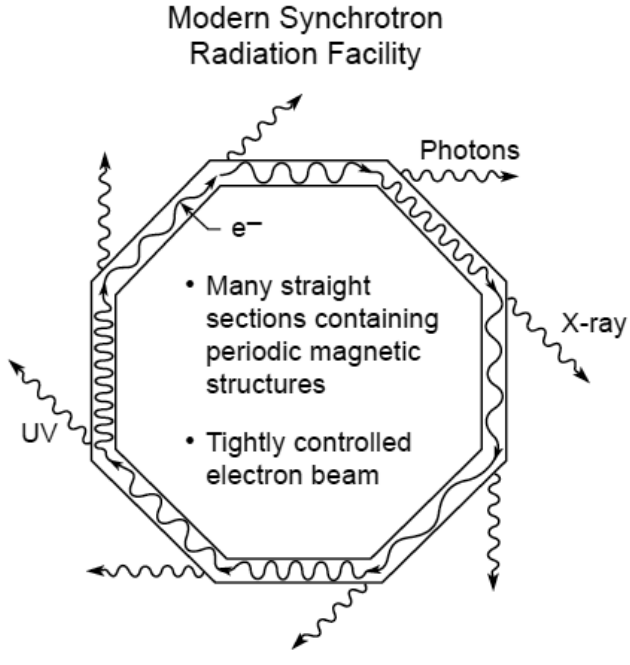

Figure 3.1. Schematic drawing of a modern synchrotron radiation facility [16]. *Published with permission from D. Attwood.*

There are basically three types of magnetic structures used to produce synchrotron radiation. Bending magnets, undulators and wigglers. Bending mag-

nets give rise to a circular electron motion leading to a broad radiation spectrum, the so-called "bending magnet radiation". In undulators there are no net deviation from a straight path of the electron motion but magnets force the electron to undulate with small amplitudes due to a comperatively weak magnetic field. The radiation is characterized by harmonic overtones and emitted with a frequency spread that can be very narrow with well-defined peaks. It is very bright and tunable. Wigglers, which are similar to undulators, but with a stronger magnetic field, radiate a spectral shape similar to that of bending magnets but shifted to higher photon energies and increased photon flux compared to bending magnets. Older types of storage rings use only bending magnet radiation but the newer so-called third generation storage rings use a combination of all three types of magnetic structures, as schematically illustrated in Fig 3.1. The latter type of light sources provide today's state-of-the-art X-rays needed for a large variety of experiments in natural sciences.

Characteristic of undulator radiation is that the angular excursions of the electrons, shown schematically in Fig 3.2, when traversing the periodic magnetic structure, are small compared to the angle of the natural radiation width. The design principle of the undulator is to arrange magnets with alternating north and south poles, illustrated by up and down arrows in Fig 3.2

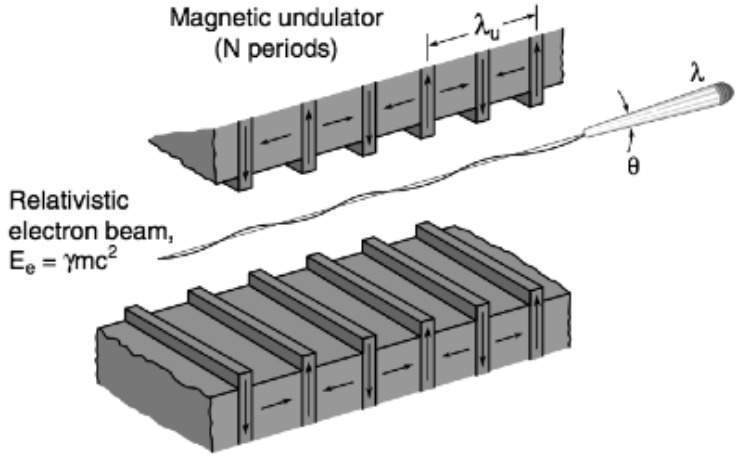

Figure 3.2. Schematic of undulator radiation [16]. *Published with permission from D. Attwood.*

When a bunch of electrons pass through the undulator they wiggle from side to side due to the alternating magnetic fields. Those fast turns produce high intensity electromagnetic radiation emitted in the forward direction of the electrons like a flash lamp conical light beam. For highly relativistic electrons, Doppler shift and Lorentz contraction reduce the observed wavelength

in the laboratory frame and the shortest wavelength is observed on the axis. Undulator periods typically measured in centimeters lead to observed x-ray wavelengths measured in Ångströms. A more detailed discussion of undulators and synchrotron radiation can be found in Ref.[15].

3.2 Beamline I411 at MAX-II

MAX II is a third-generation storage ring with a circumference of 90 m and operated at E_e = 1.5 GeV electron energy [17]. The beamline I411 is supported by a 2.65 m long undulator with 88 poles and 58.85 mm period length which produces photon energies in the range of 50-1500 eV [18]. In fig 3.3 a schematic overview of the beamline is shown.

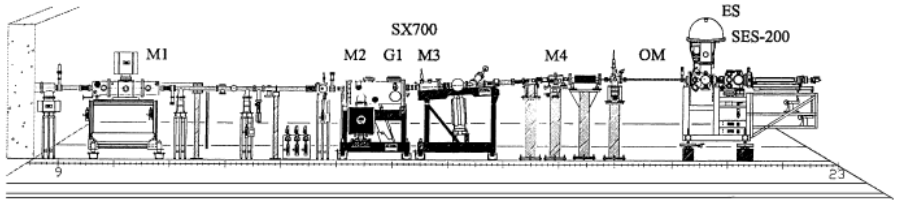

Figure 3.3. Overview of beamline I411 at MAX-lab [18].

The first optical element in the beamline is a pre-focusing optics, consisting of a cylindrical mirror (M1), horizontally focusing the radiation onto the monochromator exit slit [19]. The light is then, inside the monochromator, reflected by a plane mirror (M2) and diffracted by a plane grating (G1) with a line density of 1221 lines/mm. An elliptical mirror (M3) followed by an exit slit complete the SX 700 monochromator manufactured by Zeiss, Germany. Before the beamline terminates with a permanent end station which comprises a Scienta SES-200 hemispherical electron spectrometer (described further below), there is a re-focusing optics, consisting of a toroidal mirror (M4) that focuses the radiation onto the end station both vertically and horizontally. To achieve high photon energy resolution very small exit slit sizes, 5-20 μm, have to be used given a spot size of horizontally 0.5 mm Full Width at Half Maximum (FWHM). Vertically it is usually even less, as small monochromator exit slit sizes are mainly used [18].

3.3 Beamline U49-2 PGM-2 at BESSY-II

BESSY-II is a third-generation storage ring too, with a circumference of 240 m and operated at $E_e = 1.7$ GeV electron energy. 46 beamlines offer experimental opportunities at undulator, wiggler and dipole sources. In our work,

papers III - VI, we used the plane grating monochromator (PGM) beamline, U49/2-PGM-2 [4]. The beamline has been designed for the U49-2 undulator, which has a period length of 49.4 mm and 84 periods. The main features of the beamline can be summarized as follows [5, 20]. The first optical element is a

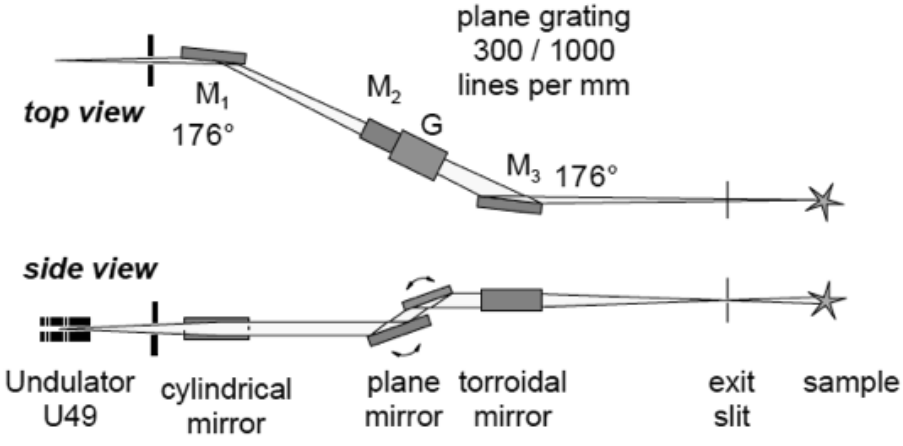

Figure 3.4. Schematic view of beamline U49-2 PGM 2 [4] *at BESSY-II* [5].

cylindrical mirror (M_1), which collimates the beam in vertical direction. This is succeeded by a plane grating monochromator, consisting of a plane mirror (M_2), two plane gratings (G) and a torroidal mirror (M_3) vertically focusing onto the exit slit, as illustrated in Fig 3.4.

The two gratings in the monochromator set up have line densities of 300 lines/mm and 1000 lines/mm, respectively, and are interchangeable, depending on the wavelength region of interest and on the resolution desired. Energies between 80-900 eV for the 300 lines/mm grating and 80-1500 eV for the 1000 lines/mm grating are accessible. The exit slit can be varied in vertical direction giving a spot size, at the sample position, of 20-200 μm (vertically) and 500 μm (horizontally). The horizontal spot size can be reduced to about 100 μm by closing a set of blends located before the (M_1) mirror.

The BESSY-II storage ring is operated in different modes, multibunch or single bunch. In single bunch mode the inter pulse time spacing is extended from 2 ns ($\cong$ 500 MHz) to 800.5 ns ($\cong$1.25 MHz) which is vital for the coincidence experiments presented in Papers III - VI.

3.4 Conventional Photoelectron Spectrometer

A conventional photoelectron spectrometer is schematically shown in Fig 3.5. Its basic principle is to focus the electron beam and then spatially disperse the electrons by their kinetic energy in a radial electrostatic field. Only electrons with kinetic energy matching the electrostatic field will pass through the electron energy analyzer and hit the detector.

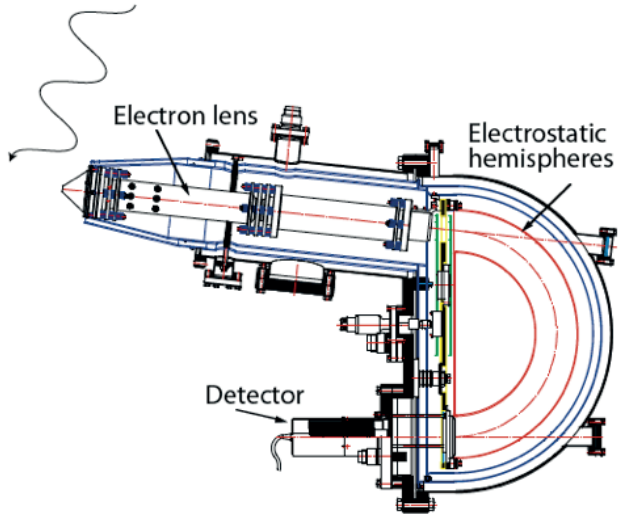

Figure 3.5. A schematic view of a Scienta photoelectron spectrometer [21]. *Published with permission from M. Lundwall.*

In the Scienta SES-200 photoelectron spectrometer [22], used in Paper I and II, the electrons are focused by an electron lens system, which also accelerates, or retards, the electrons of interest to the set pass energy of the electron energy analyser (hemispherical). Electrons with kinetic energies of about $\pm 5\%$ of the set pass energy will be detected. Hence lower pass energies results in higher energy resolution at the expense of intensity of the signal.

The resolution of the spectrometer, measured at FWHM, of the Gaussian energy distribution, is mainly depending on the spectrometer entrance slit size, s, and the pass energy E_0, and is given by

$$\text{FWHM} \approx E_0 \cdot \frac{s}{2r} \tag{3.1}$$

The pass energy is defined as the energy at which the electrons follow a central path through the spectrometer hemispheres with a mean radius r, and hit the centre of the detector. In the case of photoelectrons, the line width also depends on the bandwidth of the radiation coming from the monochromator.

In Papers I and II the calibration of the binding energy scale was made using the two narrow lines in the CS_2 spectrum with accurately determined energies of 14.4737 eV and 16.1883 eV according to the well-known valence band photoelectron spectrum [23].

3.5 Magnetic bottle time-of-flight spectrometers

3.5.1 Multi-Electron Coincidence Spectrometer

A multi-electron coincidence spectrometer, based on a magnetic bottle [6], has originally been developed in the laboratories by Prof. John H. D. Eland [7]. The magnetic bottle (see Fig 3.6) used for the work presented in Papers III - VI consists of a 2.2 m long electron flight tube which is surrounded by a solenoidal field of about 10^{-3} T, into which the divergent field of a conical permanent magnet (0.7 T at the pole), guides the electrons [24].

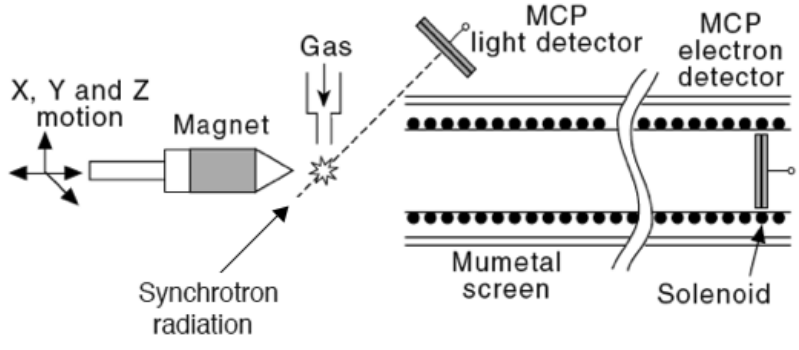

Figure 3.6. Scheme of the multi-electron coincidence spectrometer (adapted from Ref. [7])

The basis of the technique is individual electron flight time measurements and coincidence detection of electron pairs, triples etc. after photoionization [7]. Electrons are detected at the end of the flight path by a multichannel plate (MCP) detector. In a several meter long magnetic bottle, typical electron flight times are in the order of hundreds to thousands of nanoseconds. The start of the coincidence measurements can be triggered in different ways; e.g. either directly by a pulsed ionizing light source, of suitable repetition rate ($\sim$kHz) [7], or by the arrival of the first fastest electron [25], which is referenced to the ionizing pulse, as it is typically done at a synchrotron light source ($\sim$MHz repetition rate even when operated in single bunch); see also Fig 3.7. A third

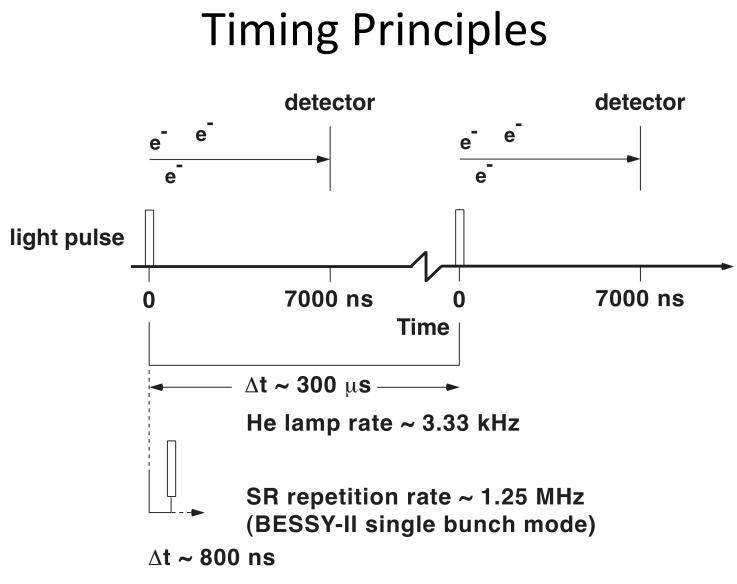

Figure 3.7. Scheme of the timing principles.

possibility is to use ion detection, as demonstrated in Paper IV. Another possibility is to use a mechanical chopper, as recently developed by our research group, to reduce the repetition rate of the synchrotron light pulse to the range of $\sim$ 10 to 120 kHz. A more detailed discussion of the chopper system can be found in Ref. [26].

3.5.2 Multi-Electron-Ion Coincidence Spectrometer

Provided that the magnetic bottle is equipped with an ion detector and that ion flight times are known from previous calibration of the ion detector, they can also be used to identify the ionizing light pulse, and hence allow for conversion of electron flight times to energies in an unambiguous way, while strongly suppressing background of false coincident electron pairs, which can be prominent in spectra measured with electrons only.

In order to detect both electrons and ions, the conical permanent magnet can be exchanged in our setup with a set of four hollow ring magnets and a soft iron pole piece, through which ions can travel in opposite direction to the electrons, as illustrated in Fig 3.8. In the experimental technique established in Paper IV, a weak continuous electrical field has been applied, in the ionization region, to extract ions from the source. The ions are accelerated further by an

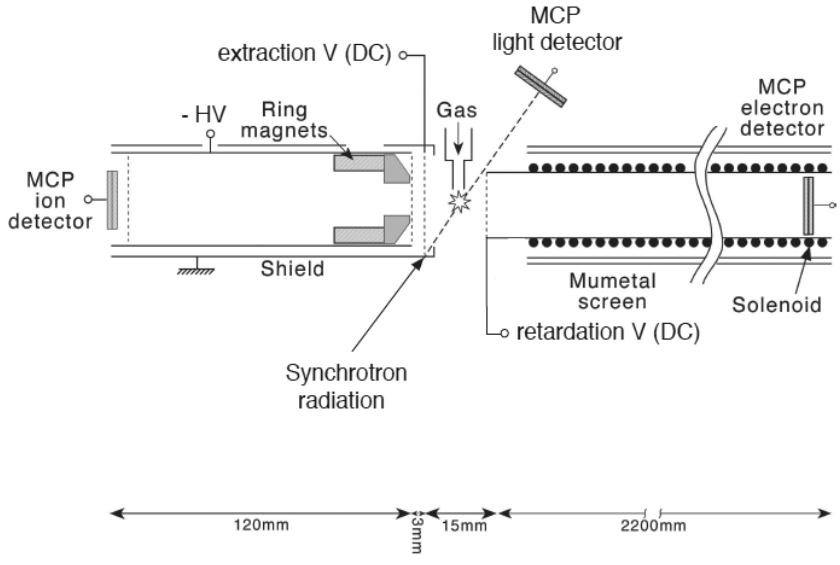

Figure 3.8. Scheme of the multi-electron-ion coincidence spectrometer (see Paper IV).

adjustable potential after passing through a first grid. The electron, ion and ring pulse (time reference) signals are recorded by a multichannel, multi-hit-time-to-digital converter, whose clock starts by the first electron to arrive from each observed event.

3.5.3 Operation principles of a magnetic bottle

To obtain good energy resolution in principle three basic conditions need to be fulfilled [6]. The magnetic field at the source must be much stronger than the homogeneous magnetic field in the flight tube to obtain parallelisation of the trajectories. Furthermore, the reduction of the field must take place in a short distance compared with the flight length to ensure a small spread in the flight times. A third condition for obtaining good energy resolution is that the relative change in the field acting on an electron during one orbit is small with respect to the total field to avoid effects of strongly nonadiabatic behaviour. This is best fulfilled for low kinetic energy electrons. In the case of higher electron energies, one needs to increase the magnetic field in the flight tube region to keep the electron trajectories near the axis. Our magnetic bottle spectrometer is designed to detect kinetic energies ranging from 0 to several hundred eV. The resolution of the instrument depends of the kinetic energy of the electrons and numerically it can be expressed for a 2.2 m instrument as the

ratio $E/\Delta E \sim 50$. For low kinetic energy electrons, less than 1 eV, the energy resolution is about 20 meV.

The sample gas is let into the interaction region by a thin needle and the light intersects the gas jet perpendicularly. The adjustable magnet (see Fig 3.6) with a conically shaped end and a fieldstrength of typically 0.7 T acts like a magnetic mirror and forces the electrons into the 2.2 m long flight tube. A solenoid surrounding the flight tube with a magnetic field much weaker, typically a few mT, guides the electrons to a micro-channel plate (MCP) detector were the electron charge gets amplified. The MCP consists of a large number of holes or channels. Every time an electron hits the inner wall of a channel it releases a large number of new electrons. Several (in our case 3) plates are configured in a stack and by applying a high voltage across the stack the electrons are accelerated towards an anode and can be registered by a time-to-digital converter. About 60% of the electrons reaching the detector are registered. Since the magnetic bottle collects about 90% of the electrons created in the interaction, this results in an overall collection-detection efficiency of about 50% of all electrons created in the ionization process.

3.6 Time to energy conversion and calibration

The flight time t of the electrons is converted to kinetic energy E_{kin} by classical mechanical considerations. Using l to denote the distance between the interaction region and the detector and assuming that the electrons fly a straight path with the electron mass m and its velocity v the following condition can be obtained

$$E_{kin} = \frac{mv^2}{2} \quad and \quad l = v \cdot t \tag{3.2}$$

Combining these two equations we obtain

$$E_{kin} = \frac{ml^2}{2t^2} \tag{3.3}$$

We can include the mass of the electron m and the distance l in a new constant called D. Adding two parameters t_0 and E_0 as calibration constants to the equation, we obtain

$$E_{kin} = \frac{D^2}{(t-t_0)^2} - E_0 \tag{3.4}$$

The values t_0 and E_0 are determined by a calibration procedure primarily using spectra lines of rare gases as references.

The equation 3.4 was used in Papers III - VI. In Papers III and IV the time-to-energy conversion was calibrated using Kr 3d photoelectron lines [27] whilst in Papers V and VI its determination was based on known energies of the Xenon atom [28].

3.7 Coincidence measurements

The aim of any coincidence experiment is to detect two or more correlated particles originating from one ionizing event. Problems that might arise in these experiments can be derived from uncorrelated particles, which randomly hit the detector, and accidentally get registered as coincidence events, giving rise to a non-statistical background. It can be electrons colliding with a surface, emission of electrons following collisions by a primary photoelectron or electrons colliding with a molecule. In order to avoid these events to some extent the gas pressure can be reduced and metal surfaces removed as far as possible from the expected electron flight paths. For highly energetic electrons the solenoid field may need to be increased. Generally speaking, it is important to reduce the background signal as much as possible since the signal from the true coincidence events is often rather weak.

There is also a statistical background caused by accidental registration of unrelated events during the same time window e.g. ionizing processes involving more than one atom. The probability of detecting n photoionization processes during the time window can be described by a Poisson distribution

$$P(n) = \frac{e^{-\lambda}\lambda^n}{n!} \tag{3.5}$$

where λ is the average number of ionized atoms per coincidence event. The background of this kind depends strongly on the kinetic energy of the electrons. On the other hand these background events can often be discarded as they violate energy conservation if assumed to originate from one single ionization event. Careful choice of photon energy and careful planning of the experiments to avoid as much as possible of the background is necessary in coincidence experiments. False coincidence events and possible ionizing events from more than one atom or molecule can further be reduced using a low detection rate at the spectrometer compared to the repetition rate of the pulsed light source used. E.g. in the experiments carried out at BESSY II, the detection rate at the spectrometer was in the kHz range whereas the synchrotron pulse repetition rate was in the MHz range.

If at least one electron in the coincidence events has a high kinetic energy, the slower electrons can be expected to be referenced to the correct light pulse i.e. the same event, assuming all electrons are detected. The so called "time window", the time interval when the electrons are detected (from the same event) is typically about 7 μs making even the low-energetic electrons to arrive at the detector. The synchrotron ring pulse period is 800.5 ns (much less than 7 μs), which means that the "first electron" arriving must have an energy about 21 eV or higher to be detected within the first ring cycle and referenced to the correct ring pulse. The "first electron" arriving at the detector triggers the time measurement start and the time for all the slower electrons in the same event are referred to the first electron. As the ring pulse is also registered by our

electronics, the flight time of the "first electron" (and all the other electrons) is absolutely determined.

4. Results

4.1 Photon absorption and cationic Rydberg states in CS_2

In a recent study of the photoelectron spectrum of the CS_2 molecule it has been found that the $S2p^{-1}$ $^2P_{3/2}$ and $^2P_{1/2}$ core hole states, observed in the 170 eV binding energy range, are bound and that the photoionization is accompanied by strong excitations of the asymmetric stretching ν_3 vibrational mode [29].

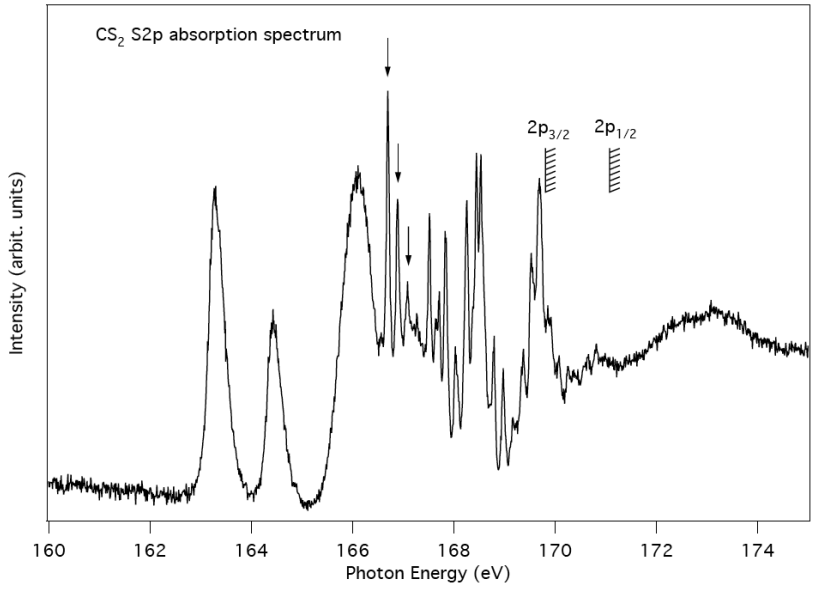

Figure 4.1. Near edge X-ray absorption spectrum of CS_2 recorded in the photon energy range $160-175$ *eV, (see Paper I).*

It seems likely that such vibrational structure could be observed also in near edge X-ray absorption spectra involving Rydberg levels close to these ionization limits, since in these cases the bonding conditions in the molecule resemble very closely those of the $S2p^{-1}$ cationic states. A high resolution absorption spectrum of CS_2 recorded in the vicinity of the sulphur 2p edges is

displayed in Fig 4.1, and its assignments are given and discussed in Paper I of this thesis.

Above the ionization limits, we could observe a resonance at a photon energy of 173.04 eV. An electron spectrum recorded at this resonance reveals sharp Auger transitions at high resolution.

One reason for carrying out this investigation was to study vibrational excitations in Rydberg states close to the S2p ionization thresholds. Another reason was to locate the energies of highly excited Rydberg states as intermediate spectator states for selected enhancement of intensities in cationic inner valence states as schematically illustrated in Fig 4.2.

Fig 4.3 shows the resonantly excited electron spectra of the CS_2 molecule in the vicinity of the S2p edge. Resonant excitations at 166.70, 166.89 and

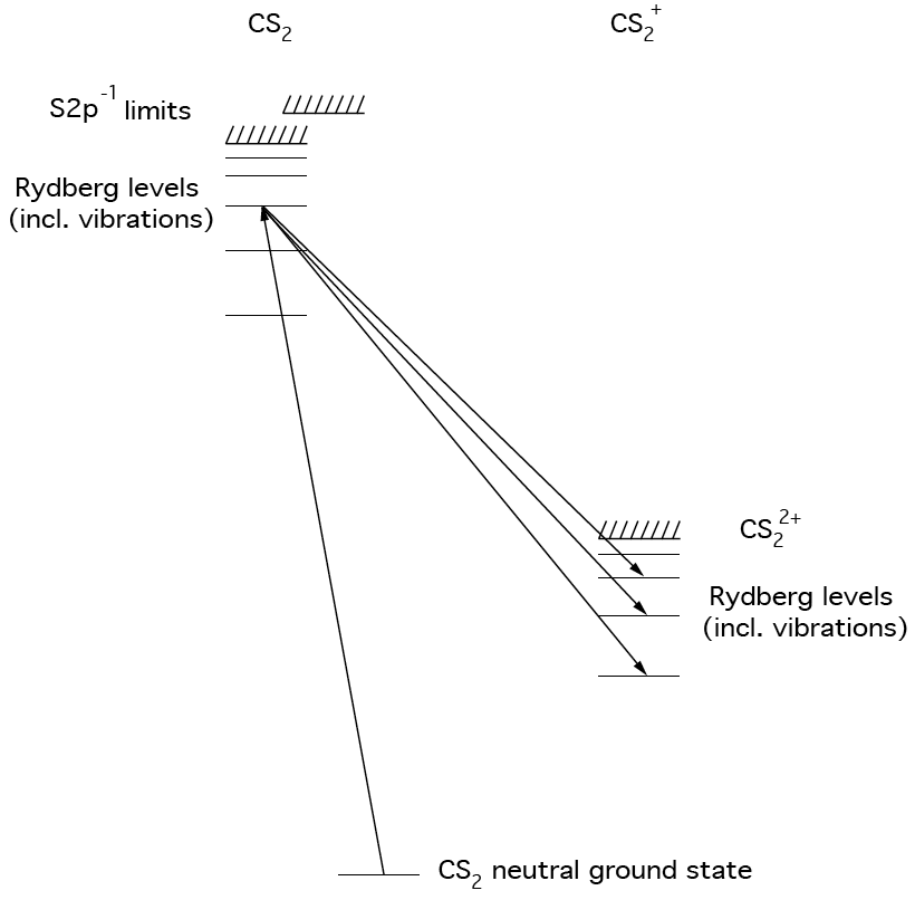

Figure 4.2. Schematic illustration of resonant core excitation to neutral intermediate Rydberg states and subsequent Auger decay to cationic Rydberg states in CS_2.

167.09 eV photon energy (marked with arrows in Fig 4.1) has been chosen

for this study. Intensive new structures appear in the $18-34$ eV binding energy range of the CS_2 electron spectra as can be seen from Fig 4.3 for the $18-25.5$ eV binding energy range. As discussed in Paper II, these spectra

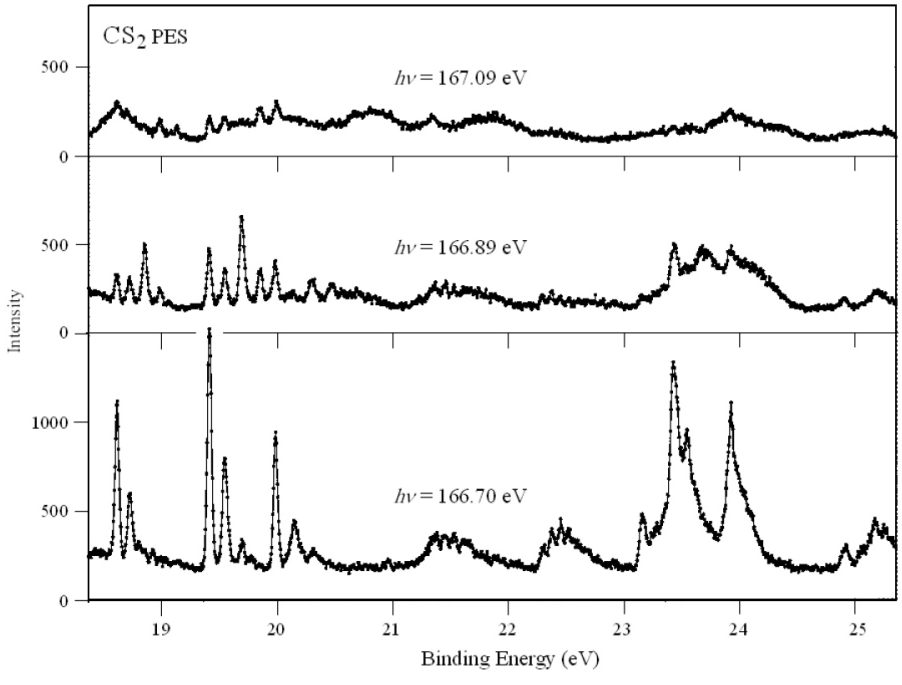

Figure 4.3. Resonant electron spectra of CS_2 *recorded using three different photon energies given in the figure (see Paper II).*

exhibit strong additional features compared to those observed in non-resonant spectra of this region [29]. A special pattern very much akin to the normal Auger decay pattern [30] is observed in these electron spectra, with energy separations between the band structures very similar to those of the Auger spectrum involving two vacancies in the dication as well as to those of the double photoionization spectrum [9]. The electron bands corresponding to two-holes-one-particle states start at 18.61 eV and cover the energy range up to about 34 eV. It is interesting that the present spectra show remarkable similarities with the double photoionization spectrum [9].

It should be mentioned that the spectra recorded at the photon energies 166.70 eV and 166.89 eV, respectively, were obtained for an energy range between 9 eV and 25.5 eV, while the spectrum obtained at 167.09 eV shows an energy range of 9 eV to about 40 eV. Hence no comparison of the spectral range above 25.5 eV binding energy can be made at the other photon energies. Further studies involving angular resolution might help to disentangle the spectral features observed above 25.5 eV. Furthermore, it is expected that,

in this energy region, intersections between potential surfaces frequently lead to predisociation. Electron-ion coincidence studies using photon energies corresponding to the resonant states could give new information related to the properties of these cationic states.

4.2 Core-valence double ionization of CS_2

Core-valence double photoionization spectra of the CS_2 molecule using photon energies in the region of 220 eV - 362.7 eV are presented in Paper III. The experiments were carried out at beam line U49/2 PGM-2 [4] of the BESSY II storage ring [5] using the magnetic bottle described in section 3.5.1. The spectra were recorded in the S2p and C1s inner-shell ionization regions and reflect dicationic states formed out of one inner-shell vacancy and one vacancy in the valence region. The flight times of two electrons originating from the same ionization process were measured. The final state electron configuration as-

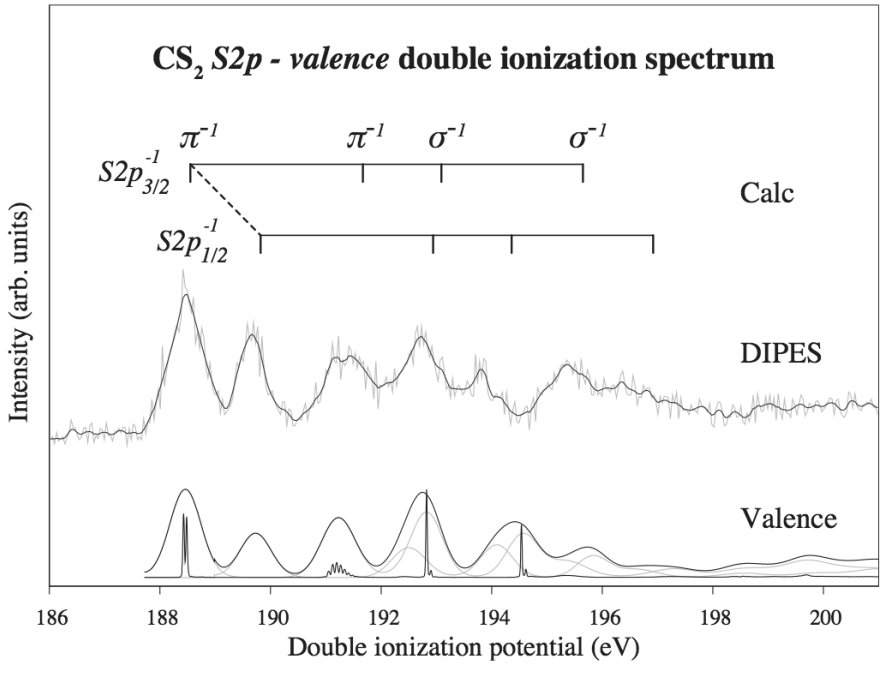

Figure 4.4. The S 2p-valence double photoionization spectrum (labelled "DIPES") of the CS_2 molecule obtained using the photon energy hν=220 eV. The interpretation given in the figure is based on the S 2p hole being either 3/2 or 1/2 coupled. A simulated spectrum (labelled "Valence") based on the UV photoelectron spectrum (narrow lines) constructed as described in the text and in Paper III is also included.

signments have been made using the generally accepted ground state valence

electron configuration of CS_2 [23, 31]

$$...(5\sigma_g)^2(4\sigma_u)^2(6\sigma_g)^2(5\sigma_u)^2(2\pi_u)^4(2\pi_g)^4$$

and presuming that the C1s and S1s, 2s and 2p inner-shell orbitals are primarily atomic-like.

Fig 4.4 shows the CS_2 S2p - valence double ionization spectrum (labelled "DIPES"), recorded at a photon energy of 220 eV. One vacancy in the S2p orbital and the other vacancy located in the valence has been created. Calculated energy levels and assignments using the MCSCF method (see Paper III), carried out by a collaborating group, are shown in the upper part. The lower part shows a simulated spectrum generated by convolving a conventional valence photoelectron spectrum (see Paper II) with two Gaussian functions separated by the S2p spin-orbit splitting of 1.27 eV [29]. The intensity ratio between the two Gaussians was 2:1 and they have a full-width-at half-maximum (FWHM) of 0.65 eV. The calculated energies and the simulated spectrum corresponds remarkably well with the measured core-valence double ionization spectrum. For further details see Paper III.

This study of the CS_2 molecule is a part of a series of investigations aiming at a better characterization of the electronic structure and interaction with radiation of this molecule and of sulfur containing molecules in general. The systematic investigation involves inner shells and valence shells as well as different charge states and different types of ionization processes including also resonant processes presented in Paper II.

4.3 Triple ionization of rare gas atoms

A new experimental technique based on a magnetic bottle [6] (cf.section 3.5.2.), using synchrotron radiation is described in Paper IV. It enables studies of valence triple ionization by soft X-ray single photon excitation. Direct valence triple photoionization spectra of Ne, Ar and Kr, not involving inner shell holes and Auger processes, are presented, and give first insight into the relative intensities of the final tricationic states observed as well as the underlying energy sharing between the three ejected electrons. As an example, the tricationic electron spectra of Ne are shown in Fig 4.5. The three low energy states ^4S, ^2D and ^2P, which arise from the valence configuration ns^2np^3, as well as two higher states, ^4P and ^2D, which arise from the ns^1np^4 configuration, are resolved. The ionization photon energy was 150 eV and 170 eV for Ne, 100 eV and 120 eV for Ar and 90 eV for Kr, respectively. All these energies are below the onset of any inner shells or near-edge structures. The spectra have been measured in coincidence with the corresponding triply charged ion, to eliminate timing uncertainties. The spectra reflect complete relative intensities of the resolved states provided that the magnetic bottle gathers essentially

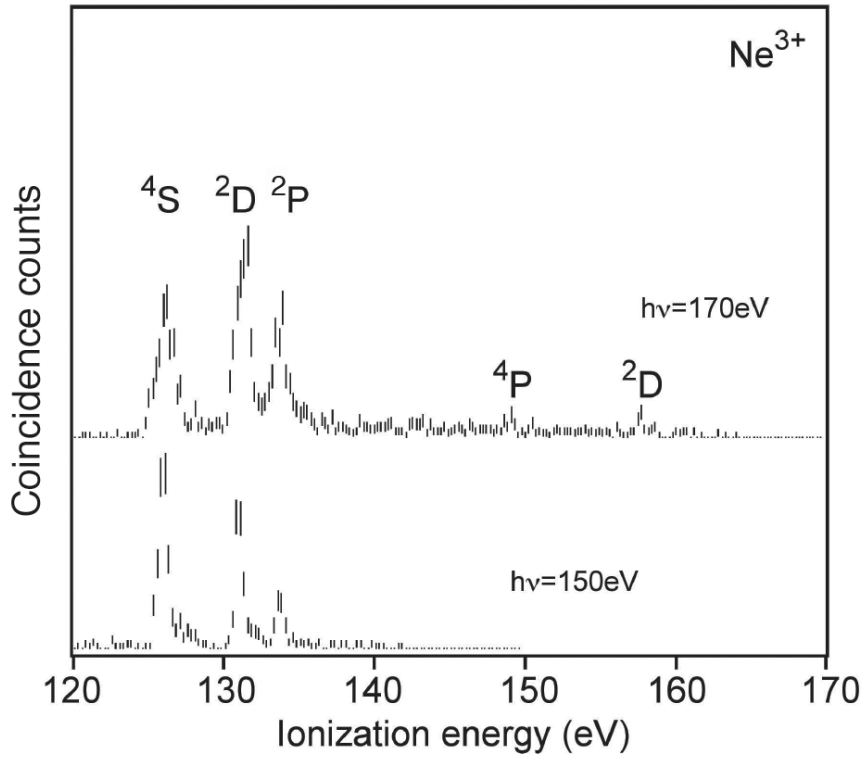

Figure 4.5. Triple photoionization spectra of Ne recorded at 150 eV and 170 eV photon energy (see Paper IV).

all electrons. As discussed in the paper, the observed intensity ratios differ from the ones expected from a statistical consideration. This suggests that both direct and indirect ionizing mechanisms are important, in particular for the lowest state of the triply charged ions.

4.4 Double core holes in molecules

The last two papers included in this thesis are studies of double core holes (DCH), created by a single photon. The two vacancies can occur either on one atom in the molecule, single-site double core holes, or on two different atoms in the molecule, two-site double core holes. Only single-site DCH are studied in this thesis.

Analysis of double core holes is demanding, because of the cross section ratio between double and single hole creation which is typically in the order of $\sim 10^{-4}$ (Paper V and VI). A careful selection of electrons is of great importance and, if available, theoretical support is here of great help. Choosing

the photon energy such that the two fastest electrons being the subsequent Auger electrons, a selection of the two slower photoelectrons coincident with the two faster Auger electrons, can be done in the energy interval defined by the Auger electrons using the analysis software developed in this thesis work. The energy sum of the two slower electrons can be plotted to show a double ionization spectrum. A map (see Fig. 4.6) is also a very good help to see if the two summed slow electrons originate from the same ionization event. If no

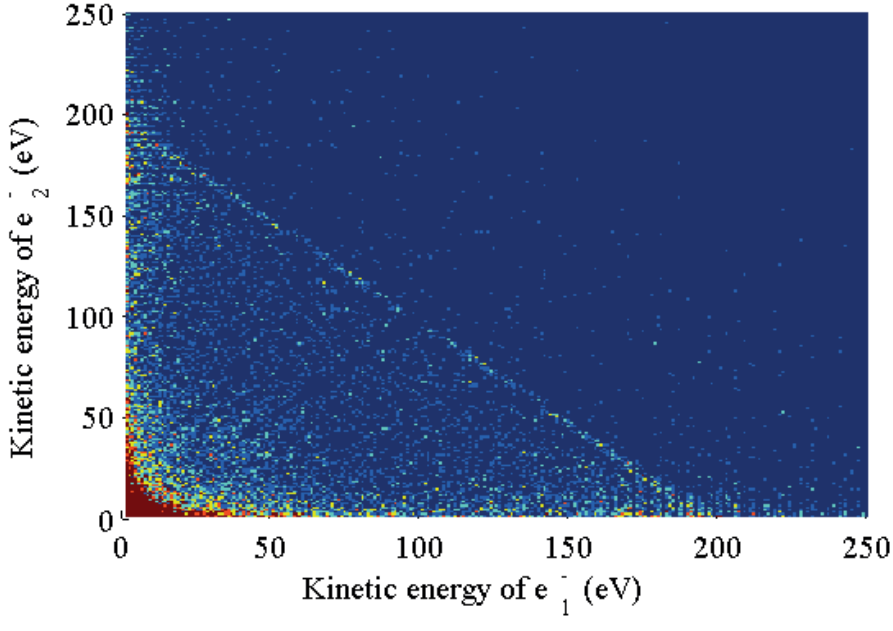

Figure 4.6. An intensity map of the N1s double ionization of NO using the photon energy 1100 eV. The horizontal and vertical axes represent the kinetic energy of either of the two N1s electrons. The data points fall on a straight line between the points at approximately (0, 195.2 eV) and (195.2, 0 eV); (see Paper V)

theoretical support is available a "rule of thumb" can be followed to find the proper energies using four electrons in coincidence. In good approximation, the double core hole energy may be at an energy ~ 2.2 times the known single core hole energy (Papers V and VI). Secondly, the energy of the first Auger electron and the second Auger electron may have a ratio of $\sim$1.2 (Papers V and VI). Finally, consideration of the final state energy must be taken into account. A schematic figure of energy levels in N_2O is shown in Fig. 4.7. It should be pointed out that the "rule of thumb" so far holds for the molecules considered in this thesis (Papers V and VI) and can expected to be a helpful tool in the analysis work of other small molecules.

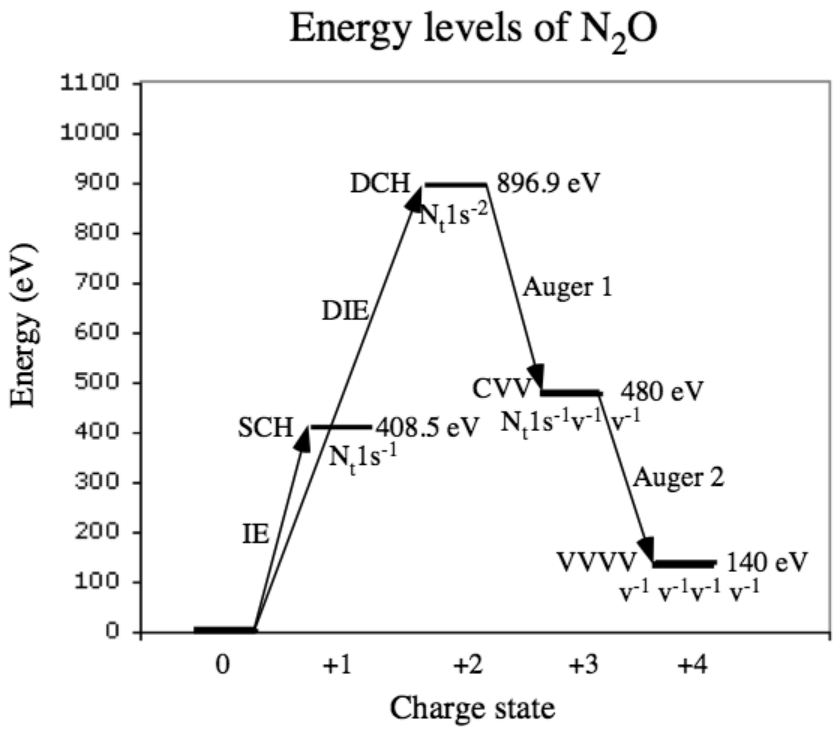

Figure 4.7. Energy levels, transitions and charge states involved in the emission of Auger electrons from N_2O after core hole production on the terminal nitrogen atom, (see Paper V).

Three molecules NO, N_2O and OCS have been studied using the magnetic bottle spectrometer, described in section 3.5.1. Four electrons were detected in coincidence (see section 3.7), two fairly slow photoelectrons and two fast Auger electrons. The photoelectrons were relatively slow because the photon energies were chosen near the double ionization limit. Generally, they share the available energy arbitrarily which is frequently found to be unequally, in particular at photon energies quite far above the double core ionization threshold, where one electron takes a higher and the other a lower energy [32]. Theoretical calculations have been carried out using Δ-self-consistent field (ΔSCF) and complete active space self-consistent field (CASSCF) techniques by theoreticians collaborating with us and are in good agreement with the experimental values.

Fig. 4.8 shows a N1s double core hole spectrum of the NO molecule recorded using the photon energy 1100 eV. One single line can be clearly observed at the binding energy 904.8 eV obtained as the energy difference between 1100 eV and the sum of the kinetic energies of the two emitted pho-

toelectrons. The corresponding coincidence map where each data point is de-

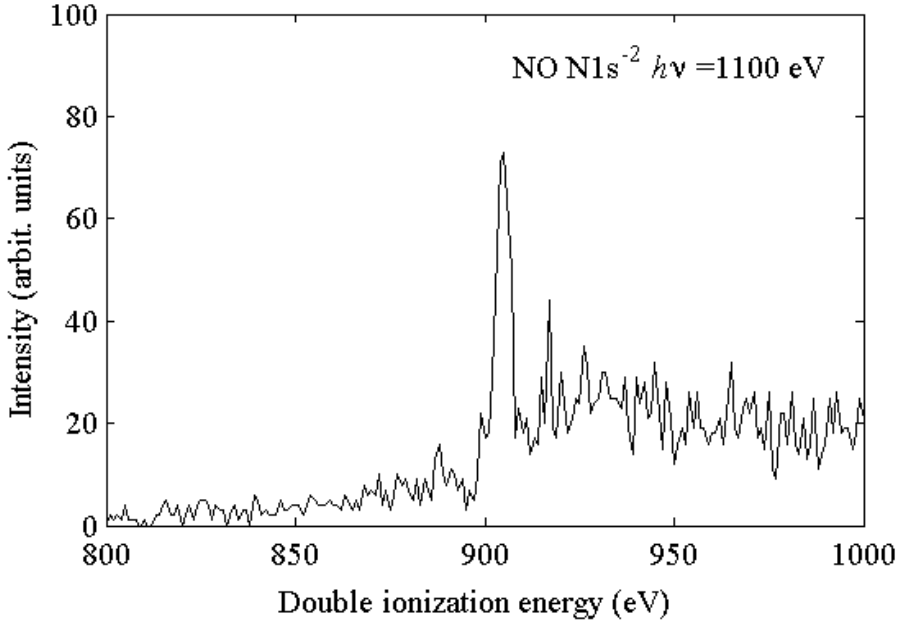

Figure 4.8. A spectrum of the N1s double ionization of NO using a photon energy 1100 eV derived from four-fold electron coincidences (see Paper V).

fined by the kinetic energies of the two core electrons, e_1 and e_2, separately represented on the horizontal and vertical axis, respectively, is shown in Fig. 4.6. As can be seen, coincidences associated with the total kinetic energy sum 195.2 eV form a clear straight line between the points on the horizontal and vertical axes with this energy. It may be noted that the distribution of excess energy between the two photoelectrons is effectively continuous with some tendency to favour pairs that have different energies, one high and one low. The core double ionization energy, DIE, revealed here is found to be 2.20 times the energy for N1s single ionization, IE (410.5 eV) [33, 34].

Similarly we have determined the DCH energies for O1s in the NO molecule and the energies of N_t1s, N_c1s and O1s in the N_2O molecule, presented in Paper V, as well as the energies for O1s, C1s and S2p in the OCS molecule, presented in Paper VI. The investigations incorporates all the "core orbitals" except S1s, for which the synchrotron radiation photon energy range available was insufficient for double photoionisation. In all cases, the ratio between the double ionization energy, DIE, and the corresponding single ionization energy, IE, is equal or close to 2.20. Studies of valence double ionization of several small molecules have given consistent ratios of DIE to IE [35], which proved useful for predictive purposes. If the ratios of DIE to IE for core holes also

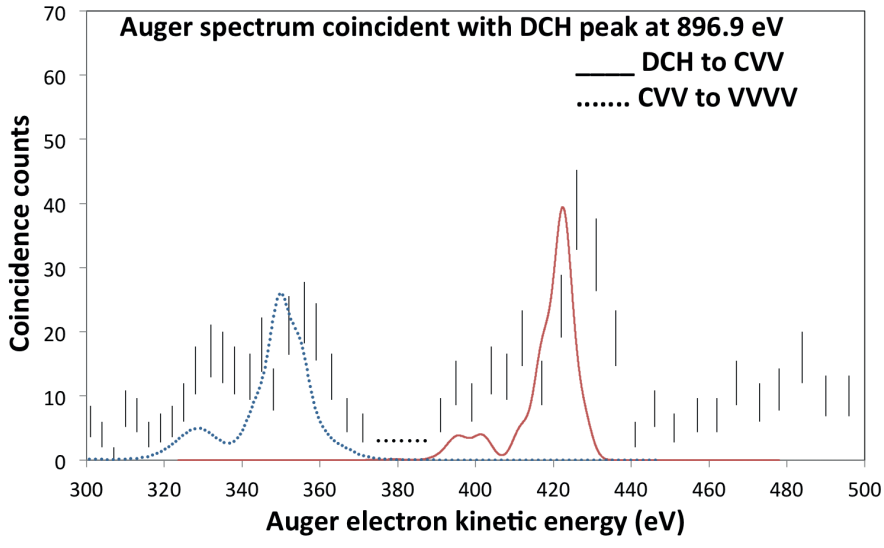

Figure 4.9. A coincident Auger spectrum of the N_2O molecule showing transitions from the double N_t1s^{-2} inner shell vacancies to final states containing four valence holes. The photon energy used to create the inner shell vacancies was 1100 eV. Dotted and solid lines show a calculated Auger electron spectrum of the N_2O molecule using the CASSCF and CASCI methods. The spectrum incorporates transitions from N_t1s^{-2} double inner shell vacancies to a final state containing four valence holes (see Paper V).

prove to be consistent over a range of molecules, they may be valuable for similar purposes.

Large chemical shifts have been observed which can be an important tool for characterization of the chemical environment and suggest that reorganisation of the electrons upon the double ionization is significant.

Auger electron spectra associated with the decay of DCHs of the N_2O molecule (Paper V) and of the OCS molecule (Paper VI) have also been obtained at photon energies 1100 eV and 1300 ev. Fig 4.9 shows an Auger electron spectrum recorded for N_2O between 300 eV and 500 eV at the photon energy 1100 eV coincident with electron pairs from creation of the initial double core hole state at 896.9 eV. The spectrum reflects transitions from the double N_t1s^{-2} inner vacancies to final states containing four valence holes. The Auger decay of DCHs may formally be presented as a two-step process. In the first step one of the core vacancies is filled by a valence electron and another valence electron is forced to leave the system denoted as DCH $\rightarrow$ CVV. In the second step the remaining core vacancy is filled by another valence electron and an additional valence electron leaves the system, which has now four valance holes denoted as CVV $\rightarrow$ VVVV. Many different final electronic states can be formed by combination of four valence holes, and all these states

are expected to contribute at well-defined energies to the spectrum shown in Fig 4.9. The hole states may involve vacancies distributed in various ways in both the outer and inner valence regions, which explains the large width of each feature, and the energies 420 eV and 340 eV represent rather average energies for the DCH $\rightarrow$ CVV and CVV $\rightarrow$ VVVV processes, respectively. An energy level diagram with the transitions and various charge states involved in the Auger process is shown previously in Fig 4.7. The broad features centered at about 400 eV and 330 eV probably reflect final states primarily connected to inner valence vacancies.

Fig. 4.10 shows the double ionization C1s spectrum of the OCS molecule using the photon energy 750 eV. This figure is included to illustrate the additional structure in all DCH spectra reported in Paper V and Paper VI. The structure tends to increase at slightly higher energy and may possibly reflect shake-up and shake-off processes but a major part is also expected to be real but unwanted coincidences with secondary electrons arising from wall collisions.

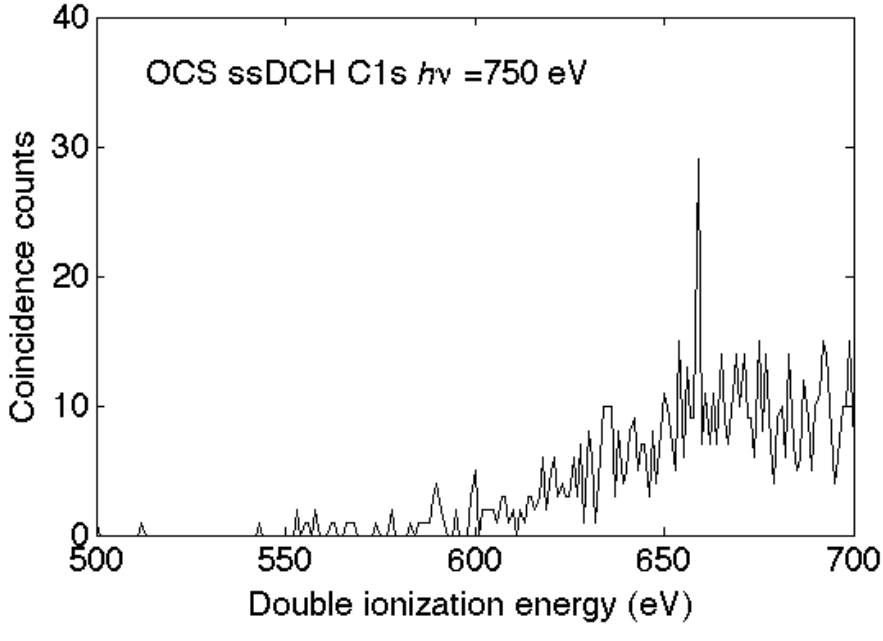

Figure 4.10. C1s double core ionization spectrum of OCS using the photon energy 750 eV (Paper VI).

Populärvetenskaplig sammanfattning på svenska (Summary in Swedish)

I avhandlingen redovisas studier på koldisulfid (CS_2), kväveoxid (NO), lustgas (N_2O) och karbonylsulfid (OCS) samt studier på ädelgaserna neon (Ne), argon (Ar) och krypton (Kr).

Genom att utsätta provgasen för exempelvis mjuk röntgenstrålning kan man från de enskilda molekylerna åstadkomma en utsändning av elektroner vars rörelseenergi speglar egenskaper hos det molekylära systemet. En teknik som använts i experimenten för att mäta rörelseenergin är att låta elektronstrålen böjas av i ett elektrostatiskt fält skapat mellan två halvsfäriska elektroder i en så kallad hemisfärisk energianalysator. Elektroner med olika energi kommer att röra sig i banor med olika radie och därmed kan deras energi bestämmas genom att de träffar detektorn på olika avstånd från ingångsspalten till analysatorn. En annan teknik, som också använts, är att mäta flygtiden för elektronerna mellan gasstrålen och detektorn i en så kallad löptidsspektrometer, där flygtiderna kan räknas om till rörelseenergi. Dessa experiment har utförts med en så kallad magnetisk flaska med ett 2,2 m långt löprör mellan gasstrålen och detektorn. Med denna metod kan man samla in de frigjorda elektronerna på ett mycket effektivt sätt, vilket har möjliggjort detektion av flera elektroner, som frigjorts vid samma fotojonisationsprocess.

Den vetenskapliga metoden som använts kallas fotoelektronspektroskopi. Den är, som framgått, baserad på fotojonisation av ett ämne och uppmätning av de frigjorda elektronernas energi. Från de uppmätta rörelseenergierna hos de frigjorda elektronerna kan den bindningsenergi med vilken de är bundna i atomen eller molekylen beräknas med hjälp av Einsteins fotoelektriska lag från 1905.

Elektroner kan frigöras från systemet på ett antal olika sätt. Först och främst kan det ske genom direkt fotojonisation, där en eller flera elektroner frigörs i en primär process utan inblandning av mellantillstånd. Ett annat sätt är genom en resonansprocess, där en elektron exciteras till en högre, icke-ockuperad energinivå (den neutrala atomen/molekylen antar ett högre energitillstånd) varifrån deexcitation till ett lägre energitillstånd sker och en eller flera elektroner lösgörs. Denna process kallas autojoinsation eller en resonant Augerövergång. Den exciterade elektronen kan besätta en valens- eller Rydbergorbital och deexcitationen av systemet kan ske genom att den exciterade elektronen deltar i övergångsprocessen (participator process) eller inte gör det (spectator process).

Om fotojonisationen sker genom att vakanser skapas i inre skal lämnas systemet i ett högt exciterat tillstånd, vilket är instabilt. När dessa vakanser utfylls av elektroner från yttre skal kan ytterligare en eller flera elektroner frigöras genom en så kallad Augerprocess. Sluttillståndet karakteriseras av en enkel- eller flerjoniserad atom eller molekyl med en eller flera vakanser i valensskal.

I de två första arbetena (Paper I och II) har elektronstrukturen för CS_2 molekylen studerats experimentellt med hjälp av en konventionell fotoelektronspektrometer försedd med en hemisfärisk elektrostatisk energianalysator. Ur de fotoelektronspektra som registrerats har bindningsenergier bestämts för såväl valensområdet som vissa inre skal. Det första arbetet avser bestämning av fotonenergier för vilka resonansfenomen uppstår i närheten av S2p-skalets jonisationsgränser. Jonisationsenergin för $S2p_{3/2,1/2}$-tillstånden är 169,806 eV respektive 171,075 eV och för att studera resonansövergångar i detta energiområde användes synkrotronstrålning vid MAX-laboratoriet i Lund med fotonenergier mellan 160 eV och 175 eV. Strax under jonisationsenergierna kunde vi observera en omfattande struktur som indikerar övergångar både till valenstillstånd och till flera Rydbergstillstånd med tillhörande finstruktur svarande mot vibrationsexcitationer med energier på ca 195 meV. Ovanför jonisationsgränsen kunde vi observera en resonans vid fotonenergin 173.04 eV. Ett elektronspektrum upptaget med hög upplösning vid den resonansen visade skarpa Augerövergångar.

I det andra arbetet användes data från spektra upptagna vid resonansenergierna 166,70 eV, 166,89 eV och 167,09 eV, motsvarande övergångar från S2p till Rydbergorbitaler i CS_2 molekylen. Deexcitationer från dessa resonanstillstånd, som tog molekylen till enkeljoniserade sluttillstånd karakteriserade av två vakanser i valensområdet och en elektron i Rydbergorbitalen (spectator processes), gav upphov till spektra som visar påtagliga likheter med dubbelt joniserade tillstånd i inre valensområdet.

I det tredje arbetet (Paper III) redovisas dubbel fotojonisation av CS_2 molekylen med skapande av en vakans i ett inre skal (S2p, C1s) och en vakans i ett valensskal. Energier rapporteras för ett antal tillstånd i energiområdet 188-200 eV (S2p) samt i energiområdet 310-320 eV (C1s) och tolkningar av spektra har kunnat göras med hjälp av beräkningsresultat erhållna med en MCSCF-metod.

Det fjärde arbetet (Paper IV) är en studie av trefaldig fotojonisation av ädelgaserna Ne, Ar och Kr. Sannolikheten för sådana processer är mycket låg och motsvarande linjer i spektra är svaga i jämförelse med den bakgrund som alltid finns. Vi utnyttjade därför möjligheten att koppla en jondetektor till spektrometern så att elektronerna kunde detekteras i koincidens med jonen. Därmed kunde vi erhålla en mer väldefinierad startpuls (jonen) som på ett bättre sätt säkerställde från vilken jonisationshändelse elektronerna kom, och på detta sätt underlättades tolkningen av spektra.

Arbetena fem och sex (Papers V and VI) behandlar dubbla "core-hål", där två vakanser skapas i inre skal av en infallande foton. Arbete fem är en studie av molekylerna NO och N_2O med initialvakanser i O1s och N1s medan arbete

VI gäller molekylen OCS med vakanser i O1s, C1s och S2p. Genom den direkta fotojonisationen frigörs två fotoelektroner och ett mycket högt exciterat mellantillstånd uppstår i den dubbelt joniserade molekylen. Detta tillstånd har kort livstid, och det sönderfaller oftast genom Augerövergångar till nya tillstånd hos systemet. Man kan betrakta sönderfallet som en tvåstegsprocess där två valenselektroner successivt fyller "core"-vakanserna. Vid den första Augerövergången fylls den ena vakansen och en valenselektron frigörs, och vid den andra Augerövergången fylls den kvarvarande vakansen av en ny valenselektron samtidigt som ännu en valenselektron tvingas ut från systemet. Sluttillståndet för systemet är då en fyrfaldigt joniserad molekyl och fyra fria elektroner, två fotoelektroner och två Augerelektroner. Studierna har utförts så att initialvakanserna alltid har funnits på samma atom och i samma orbital (single site double core hole). Tvärsnitten för skapande av dubbelvakanserna är alltid låga, omkring $1{:}10^{-4}$ jämfört med en enkelvakans (single core hole), vilket innebär att i ca 10 000 signaler ska det finnas en som svarar mot en dubbelvakans. Genom att utnyttja möjligheten till detektion av de fyra elektronerna i koincidens kan den identifieras. De två fotoelektronerna delar på den tillgängliga energin på så sätt att alla möjligheter förekommer men med viss favorisering för en snabb och en långsam elektron. Genom att fotonenergin vanligen väljs så att den ligger strax ovanför tröskeln för dubbel fotojonisation (för att få så bra upplösning som möjligt) har de två Augerelektronerna i allmänhet mycket högre rörelseenergi och därmed kortare tid fram till detektorn än fotoelektronerna. Analysen görs då utgående från de "snabba" Augerelektronerna och sedan konstrueras ett fotoelektronspektrum utifrån de fotoelektroner som detekteras i koincidens med Augerelektronerna. Villkoret är att alla fyra elektronernas sammanlagda energi, minus energin för skapande av de fyra vakanserna som karakteriserar sluttillståndet för molekylen, skall överensstämma med energin hos den infallande fotonen.

Acknowledgments

I wish to express my deep gratitude to my main supervisor Raimund Feifel for his most inspiring leadership and unfailing generous support during the course of this work.
I would like to thank as well my assistant supervisor Leif Karlsson who gave me inspiration and courage to continue with research, after finishing the exam work, and with a never-failing patience with all my questions.
I also wish to thank my assistant supervisor Jan-Erik Rubensson who spared me much of his time in instructive and interesting discussions as well as I wish to thank my former assistant supervisor Joseph Nordgren.
It has been a great privilege to work with John Eland from Oxford University to whom I am very grateful.
It is a great pleasure to acknowledge generous assistance with computer programming and interesting discussions by Kjell Pernestål.
Many thanks to my roommate Carl Caleman for interesting discussions and pleasant fellowship.
I owe Johan Larsson, Filip Heijkenskjöld, Staffan Andersson, Egil Andersson, Pelle Linusson, Melanie Mucke, Rein Maripuu and Martin Berglund many thanks for kind and interesting collaboration and Vitali Zhaunerchyk for teaching me the MatLab world.
I also owe Karl-Einar Ericsson many thanks for all help with the computer programs and Åsa Andersson as well as Anne Kronquist for generous help when I have been lost in administrative issues.
The friendly assistance from the staff of the Department of Physics and Astronomy is gratefully acknowledged.
I also would like to thank our collaborative group in theoretical calculations, who supported strongly the data interpretation.
Many thanks to principal Jörgen Norman and the management team at Celsiusskolan for understanding my situation in combining teaching with research.

And last but not least a huge thank you to my Carina.

Uppsala, March 2014

Lage Hedin

References

[1] Kai Siegbahn et al., ESCA: Atomic, Molecular and Solid State Structure Studied by means of Electron Spectroscopy, Almqvist & Wiksell, Uppsala 1967.

[2] Kai Siegbahn et al., ESCA applied to Free Atoms and Molecules, North-Holland Publ. Co 1969.

[3] J.H.D. Eland, *Adv. Chem. Phys.* **141**, 103 (2009)

[4] D. R. Batchelor, R. Follath, and D. Schmeisser, *Nucl. Instrum. Methods Phys. Res. A* **467-468**, 470 (2001).

[5] http://www.bessy.de/

[6] P. Kruit and F.H. Read, *J. Phys. E* **16**, 313 (1983).

[7] J.H.D. Eland, O. Vieuxmaire, T. Kinugawa, P. Lablanquie, R. I. Hall and F. Penent, *Phys. Rev. Lett.* **90**, 053003 (2003).

[8] J.H.D. Eland, S.S.W. Ho and H.L. Worthington, *Chem. Phys.* **290** 27 (2003).

[9] J.H.D. Eland, *Chem. Phys.* **294** 171 (2003).

[10] R. Feifel and M.N. Piancastelli, *J. Electron Spectrosc. Relat. Phenom.* **183**, 10 (2011).

[11] U. Ankerhold, B. Esser and F. von Busch, *Chem. Phys.*. **220**, 393 (1997).

[12] E.U. Condon, *Phys. Rev.* **32**, 858 (1928).

[13] M. Born and R. Oppenheimer, *Ann. Phys.* **84**, 457 (1927).

[14] J. Schirmer, L.S. Cederbaum, W. Domcke and W. von Niessen, *Chem. Phys.* **26**, 149 (1977).

[15] D. Attwood, Soft x-rays and Extreme Ultraviolet Radiation. Principles and Applications. CUP (1999).

[16] http://www.coe.berkeley.edu/AST/sxreuv/
D. Attwood, *Lecture material used in class: 9. Introduction to Synchrotron Radiation, Bending Magnet Radiation* page 8 and 18

[17] http://www.maxlab.lu.se/

[18] M. Bässler, A. Ausmees, M. Jurvansuu, R. Feifel, J.-O. Forsell, P. de Tarso Fonseca, A. Kivimäki, S. Sundin, S.L. Sorensen, R. Nyholm, O. Björneholm, S. Aksela and S. Svensson,
Nucl. Instrum. Methods A **469**, 382 (2001).

[19] R. Nyholm, S. Svensson, J. Nordgren and A. Flodström, *Nucl. Instrum. Methods A* **246**, 267 (1986).

[20] K.J.S. Sawhney, F. Senf and W. Gudat, *Nucl. Instrum. Methods Phys. Res. A* **467-468**, 466 (2001).

[21] M. Lundwall PhD thesis ISBN 978-91-554-6769-2 (2007).

[22] N. Mårtensson, P. Baltzer, P.A. Brühwiler, J.-O. Forsell, A. Nilsson, A. Stenborg and B. Wannberg, *J. Electron Spectrosc. Relat. Phenom.* **70**, 117 (1994).

[23] P. Baltzer, B. Wannberg, M. Lundqvist, L. Karlsson, D. M. P. Holland, M. A. MacDonald, M. A. Hayes P. Tomasello, and W. von Niessen, *Chem. Phys.* **202**, 185 (1996).

[24] John H.D. Eland and R. Feifel, *Chem. Phys.* **327**, 85 (2006).

[25] F. Penent, J. Palaudoux, L. Andric, P. Lablanquie, R. Feifel and J.H.D. Eland, *Phys. Rev. Lett*. **95**, 083002 (2005).

[26] S. Plogmaker, P. Linusson, J.H.D. Eland, N. Baker, E.M.J. Johansson, H. Rensmo, R. Feifel and H. Siegbahn, *Rev. Sci. Instrum*. **83**, 013115 (2012).

[27] Z.-S. Yuan, L.-F. Zhu, X.-J. Liu, W.-B. Li, H.-D. Cheng, J.-M. Sun, and K.-Z. Xu, *Phys. Rev. A* **71**, 064701 (2005).

[28] T.X. Carroll et al., *J. Elec. Spec. Rel. Phen.* **125**, 127 (2002).

[29] H. Wang, M. Bässler, I. Hjelte, F. Burmeister, L. Karlsson, *J. Phys. B: At. Mol. Opt. Phys.* **34**, 1745 (2001).

[30] U. Alkemper and F. von Busch, *J. Electron Spectrosc. Relat. Phenom.* **93**, 115 (1998).

[31] K. Kimura, S. Katsumata, Y. Achiba, T. Yamazaki, and S. Iwata, *Handbook of HeI Photoelectron Spectra of Fundamental Organic Molecules* (Japan Scientific, Tokyo, Halsted Press, New York, 1981).

[32] P. Lablanquie, *et al., Phys. Rev. Lett*. **106**, 063003 (2011).

[33] H.W. Chen, W.L. Jolly, S.F. Xiang, and P. Legzdins, *Inorg. Chem*. **20**, 1779 (1981).

[34] A.A. Bakke, A.W. Chen and W.L. Jolly, *J. Electron Spectrosc. Relat. Phenom.* **20**, 333 (1980).

[35] R.D. Molloy, A. Danielsson, L. Karlsson, and J. H. D. Eland, *Chem. Phys.* **335**, 49 (2007).

Acta Universitatis Upsaliensis

Digital Comprehensive Summaries of Uppsala Dissertations from the Faculty of Science and Technology 1132

Editor: The Dean of the Faculty of Science and Technology

A doctoral dissertation from the Faculty of Science and Technology, Uppsala University, is usually a summary of a number of papers. A few copies of the complete dissertation are kept at major Swedish research libraries, while the summary alone is distributed internationally through the series Digital Comprehensive Summaries of Uppsala Dissertations from the Faculty of Science and Technology. (Prior to January, 2005, the series was published under the title "Comprehensive Summaries of Uppsala Dissertations from the Faculty of Science and Technology".)

Distribution: publications.uu.se
urn:nbn:se:uu:diva-221128

ACTA
UNIVERSITATIS
UPSALIENSIS
UPPSALA
2014